



# Identification of Dynamic Models of Marine Structures from Frequency-domain Data Enforcing Model Structure and Parameter Constraints

Technical Report: 2009-01.0-Marine Systems Simulator

Sept 2009

Tristan Perez<sup>1,3</sup> Thor I. Fossen<sup>2,3</sup>

<sup>1</sup>*Centre for Complex Dynamic Systems and Control (CDSC), The University of Newcastle, Callaghan, NSW-2308, AUSTRALIA. E-mail: Tristan.Perez@newcastle.edu.au*

<sup>2</sup>*Department of Engineering Cybernetics, Norwegian University of Science and Technology, N-7491 Trondheim, Norway. E-mail: Fossen@ieee.org*

<sup>3</sup>*Centre for Ships and Ocean Structures (CeSOS) Norwegian University of Science and Technology, N-7491 Trondheim, Norway.*

## Contents

<b>1</b>	<b>Introduction</b>	<b>4</b>
<b>2</b>	<b>A Linear Model based on the Cummins Equation</b>	<b>4</b>
<b>3</b>	<b>Frequency-domain Representation—Non-Parametric Models</b>	<b>5</b>
<b>4</b>	<b>Parametric Approximations</b>	<b>6</b>
<b>5</b>	<b>Constraints on Parametric Approximations</b>	<b>8</b>
<b>6</b>	<b>Assessing the Quality of the Model</b>	<b>9</b>
<b>7</b>	<b>Some Aspects of Time-domain Identification of Fluid Memory Functions</b>	<b>10</b>
<b>8</b>	<b>Frequency-domain Identification of Fluid-memory Models</b>	<b>11</b>
8.1	Complex Curve Fitting Revisited . . . . .	11
8.2	A Linearised Iterative Solution for Complex Curve Fitting . . . . .	12
8.3	Practical Issues Associated with the Identification of Fluid-memory Approximations . . . . .	13
8.3.1	Preparing the Data . . . . .	13
8.3.2	Adding Prior Knowledge . . . . .	14
8.3.3	Order selection . . . . .	15
8.3.4	Stability . . . . .	15
8.3.5	Passivity . . . . .	15
8.4	A practical Algorithm for the Identification Fluid-memory Models . . . . .	16
<b>9</b>	<b>Joint Identification of Infinite-frequency Added Mass and Fluid Memory Models</b>	<b>17</b>
<b>10</b>	<b>Application Examples</b>	<b>18</b>
10.1	Identification of Fluid-memory models of a Semi-submersible. . . . .	18
10.2	Identification of the Joint Infinite-frequency Added Mass and Fluid-memory models of a FPSO. . . . .	18
<b>11</b>	<b>Conclusions</b>	<b>19</b>
<b>A</b>	<b>Properties of the Fluid Memory Models</b>	<b>22</b>
A.1	Initial-Time Value . . . . .	22
A.2	Final-Time Value . . . . .	22
A.3	Low-frequency Asymptotic Value . . . . .	22
A.4	High-frequency Asymptotic Value . . . . .	23
A.5	Passivity . . . . .	23

## Replacements

This is a new technical report.

## Executive summary

Linear time-domain seakeeping models can be approximated by finite-dimensional time-invariant models obtained from data computed by hydrodynamic codes. Different proposals have appeared in the literature to address the identification problem in both time and frequency domain. This report concentrates on the latter and, it addresses the issue of using constraints on model structure and parameters to refine the search of approximating parametric models. The constraints are derived from the hydrodynamics and represent prior information for the identification process.

Hydrodynamic properties of the models are reviewed and their consequences on parametric model approximations discussed. Then, two related frequency-domain identification problems with constraints are considered in detail. The first problem is that of identifying the fluid-memory terms in the Cummins equation with knowledge of infinite frequency added mass. The second problem arises from the use of 2D hydrodynamic data, which do not provide the infinite-frequency added mass. The second problem can be formulated as an extension of the first. Therefore, identification problems using either 3D or 2D hydrodynamic data can be considered within the same framework. Practical issues associated with the identification are discussed, and a detailed description of the proposed algorithms is presented. The quality of the models obtained with the proposed algorithm are illustrated using data of a semi-submersible and a FPSO.

## 1 Introduction

Linear models for the description of rigid-body motion of marine structures are the basis of training simulators, hardware in the loop testing simulators, and analysis and design of motion control systems. Once a linear model is obtained, nonlinear terms can be added to improve the quality of the model depending on its particular use. One approach to develop linear time-domain models of marine structures consist of using potential theory to compute frequency-dependent coefficients and frequency responses, and then use these data to either implement the Cummins equation or to apply system identification to obtain a model that approximates the Cummins equation. The latter has advantages with respect to analysis and simulation speed, which can improve up to two orders of magnitude depending on number of degrees of freedom considered (Taghipour et al., 2008). A great deal of work has been reported in the literature proposing the use of different identification methods to obtain approximating models—see, for example, Jefferys et al. (1984), Jefferys and Goheen (1992), Yu and Falnes (1995), Yu and Falnes (1998), Holappa and Falzarano (1999), Hjulstad et al. (2004), Kristansen and Egeland (2003), Kristiansen et al. (2005), Jordan and Beltran-Aguedo (2004), McCabe et al. (2005), and Sutulo and Guedes-Soares (2005).

The approximating models obtained may not necessarily satisfy all the properties of the Cummins equation unless appropriate constraints on the model are used. From potential theory, various properties of the Cummins equation can be derived: stability, passivity, and time-frequency-domain asymptotic properties. These properties can be used to set constraints on the structure and parameters of the approximating models. The use of constraints in the identification process refines the search for models and improves the quality of the approximations.

In this paper, we review the properties of the Cummins equation in relation to the constraints that they impose on parametric model approximations for fluid memory models. We then propose two frequency-domain identification algorithms that use the constraints. The proposed algorithms take into account the identification based on 3D and 2D frequency-domain data. Hydrodynamic data based on 2D-potential theory can be used for slender structures. Codes that compute 2D data do not provide the infinite-frequency added mass coefficients. Hence, we discuss an extension to the identification problem that uses 3D data, such that identification problems using either 3D or 2D data are considered within the same framework.

## 2 A Linear Model based on the Cummins Equation

The linearised equation of motion of marine structure can be formulated as

$$\mathbf{M}_{RB} \ddot{\boldsymbol{\xi}} = \boldsymbol{\tau}. \quad (1)$$

The matrix  $\mathbf{M}_{RB}$  is the rigid-body generalised mass. The generalised-displacement vector  $\boldsymbol{\xi} \triangleq [x, y, z, \phi, \theta, \psi]^T$  gives the position of the body-fixed frame with respect to an equilibrium frame ( $x$ -surge,  $y$ -sway, and  $z$ -heave) and the orientation in terms of Euler angles ( $\phi$ -roll,  $\theta$ -pitch, and  $\psi$ -yaw). The generalised force vector and  $\boldsymbol{\tau} \triangleq [X, Y, Z, K, M, N]^T$  gives the respective forces and moments in the six degrees of freedom. This force vector can be separated into three components:

$$\boldsymbol{\tau} = \boldsymbol{\tau}_{rad} + \boldsymbol{\tau}_{res} + \boldsymbol{\tau}_{exc}, \quad (2)$$

where the first component corresponds to the radiation forces arising from the change in momentum of the fluid due to the motion of the structure, the second are restoring forces due to gravity and buoyancy, and the third component represents the pressure forces due to the incoming waves.

Cummins (1962) studied the radiation hydrodynamic problem in an ideal fluid in the time-domain and found the following representation for linear the pressure forces:

$$\boldsymbol{\tau}_{rad} = -\mathbf{A}_{\infty} \ddot{\boldsymbol{\xi}} - \int_0^t \mathbf{K}(t-t') \dot{\boldsymbol{\xi}}(t') dt'. \quad (3)$$

The first term in (3) represents pressure forces due the accelerations of the structure, and  $\mathbf{A}_{\infty}$  is a constant positive-definite added mass matrix. The second term represents fluid-memory effects that capture the energy transfer from the motion of the structure to the radiated waves. The convolution term is known as a *fluid-memory model*. The kernel of the convolution term,  $\mathbf{K}(t)$ , is the matrix of *retardation* or *memory functions* (impulse responses).

By combining terms and adding the linearised restoring forces  $\boldsymbol{\tau}_{res} = -\mathbf{G}\boldsymbol{\xi}$ , the *Cummins Equation* (Cummins, 1962) is obtained:

$$(\mathbf{M}_{RB} + \mathbf{A}_{\infty}) \ddot{\boldsymbol{\xi}} + \int_0^t \mathbf{K}(t-t') \dot{\boldsymbol{\xi}}(t') dt' + \mathbf{G}\boldsymbol{\xi} = \boldsymbol{\tau}_{exc}, \quad (4)$$

Equation (4) describes the motion of the structure for any wave excitation  $\boldsymbol{\tau}_{exc}(t)$  provided the linearity assumption is satisfied; and it forms the basis of more complex models, which can be obtained by adding non-linear terms to represent different physical effects such as viscous damping, and non-linear restoring terms due to mooring lines.

### 3 Frequency-domain Representation—Non-Parametric Models

When the radiation forces (3) are considered in the frequency domain, they can be expressed as follows (Newman, 1977; Faltinsen, 1990):

$$\boldsymbol{\tau}_{rad}(j\omega) = -\mathbf{A}(\omega) \ddot{\boldsymbol{\xi}}(j\omega) - \mathbf{B}(\omega) \dot{\boldsymbol{\xi}}(j\omega). \quad (5)$$

The parameters  $\mathbf{A}(\omega)$  and  $\mathbf{B}(\omega)$  are the frequency-dependent added mass and potential damping respectively. This representation leads to the following frequency-domain relationship between the excitation forces and the displacements:

$$[-\omega^2[\mathbf{M} + \mathbf{A}(\omega)] + j\omega\mathbf{B}(\omega) + \mathbf{G}]\boldsymbol{\xi}(j\omega) = \boldsymbol{\tau}_{exc}(j\omega). \quad (6)$$

Ogilvie (1964) showed the relation between the parameters of the time-domain model (4) and frequency-domain model (6) using the Fourier Transform of (4):

$$\mathbf{A}(\omega) = \mathbf{A}_{\infty} - \frac{1}{\omega} \int_0^{\infty} \mathbf{K}(t) \sin(\omega t) dt, \quad (7)$$

$$\mathbf{B}(\omega) = \int_0^{\infty} \mathbf{K}(t) \cos(\omega t) dt. \quad (8)$$

From expression (7) and the application of the Riemann-Lebesgue lemma, it follows that  $\mathbf{A}_{\infty} = \lim_{\omega \rightarrow \infty} \mathbf{A}(\omega)$ , and hence  $\mathbf{A}_{\infty}$  is called infinite-frequency added mass.

It also follows from the Fourier transform that the time- and frequency-domain representation of the retardation functions are

$$\mathbf{K}(t) = \frac{2}{\pi} \int_0^{\infty} \mathbf{B}(\omega) \cos(\omega t) d\omega, \quad (9)$$

and

$$\mathbf{K}(j\omega) = \int_0^\infty \mathbf{K}(t)e^{-j\omega t} dt = \mathbf{B}(\omega) + j\omega[\mathbf{A}(\omega) - \mathbf{A}_\infty]. \quad (10)$$

Expressions (9) and (10) are key to generate the data used in the identification problems that seek parametric approximations to the fluid memory terms.

Hydrodynamic codes based on potential theory, are nowadays readily to compute  $\mathbf{B}(\omega)$  and  $\mathbf{A}(\omega)$  for a finite set of frequencies of interest—see, for example, Beck and Reed (2001) for an overview of the characteristics of these codes. Hydrodynamic codes based on 3D potential theory also solve the boundary-value problem associated with infinite-frequency that gives  $\mathbf{A}_\infty$ .

Potential theory codes have their inherent limitations due to theoretical and implementation issues, which limit the lowest and the highest frequencies that can be computed. For 3D codes based on low-order panel methods, it is generally accepted that the characteristic size of the panels should be of the order of 1/10 of the shortest wave length used in the computations (Faltinsen, 1990), whereas for high order panel methods, sizes of 1/4 of the shortest wave length are usually appropriate. This characteristic limits the upper frequency since smaller panels increase the number of computations significantly and may result in numerical problems. For slender vessels, codes based on strip theory (2D) can be used. Slenderness results in the velocity field being nearly constant along the longitudinal direction, and this characteristic allows reducing the 3D problem to a 2D problem (Newman, 1977). These codes have a limit on the lower frequency—this is due to an assumption made on the free surface condition that results in a simplification of the boundary-value problem (Salvesen et al., 1970). The two-dimensional hydrodynamic problem associated with each section or strip of the hull can be solved, for example, using conformal mapping or panel methods. If the 2D code uses panel methods to compute the hydrodynamic parameters associated with each strip, then the same limitations for high frequencies discussed for the 3D codes hold. Strip theory codes do not compute the zero and infinite frequency cases.

## 4 Parametric Approximations

A direct approach to use non-parametric models to implement simulation models consists of a direct implementation of (4) in discrete time. This approach can be time consuming and may require significant amounts of computer memory. In addition, the non-parametric models can result difficult to work with for the analysis and design of vessel motion control systems.

One way to overcome these difficulties consists of approximating the fluid-memory models by a linear-time-invariant parametric model in state-space form:

$$\boldsymbol{\mu} = \int_0^t \mathbf{K}(t-t')\dot{\boldsymbol{\xi}}(t') dt' \approx \begin{cases} \dot{\mathbf{x}} = \hat{\mathbf{A}}\mathbf{x} + \hat{\mathbf{B}}\dot{\boldsymbol{\xi}} \\ \hat{\boldsymbol{\mu}} = \hat{\mathbf{C}}\mathbf{x} + \hat{\mathbf{D}}\dot{\boldsymbol{\xi}}, \end{cases} \quad (11)$$

where the number of components of the state vector  $\mathbf{x}$  corresponds to the order of the approximating system and the matrices  $\hat{\mathbf{A}}$ ,  $\hat{\mathbf{B}}$ ,  $\hat{\mathbf{C}}$ , and  $\hat{\mathbf{D}}$  are constants.

From a simulation point of view, the advantage of the state-space model on the right-hand side of (11) lies in the Markovian property of the model: at any time instant, the values of the state  $\mathbf{x}$  summarise all the past information of the system. Hence, it is only necessary to store the state vector

of the model. Taghipour et al. (2008), considered as an example a time-domain model corresponding to the vertical motion of a container ship (4 convolutions—coupled heave-pitch), and obtained increases in simulation speed of 40 times when using state-space models with respect to models using direct convolution integration. Similarly, Taghipour et al. (2007), showed an increase in simulation speeds of 80 times for a flexible structure. The gain in simulation speed becomes more significant as the complexity of the model increases.

The approximating state-space model for the convolution term can be obtained using system identification. For this particular application, the identification procedure can be separated into the following steps:

1. Compute the data for identification.
2. Determine the structure and order of a parametric approximating model.
3. Estimate the parameters.
4. Evaluate the quality of the model and assess if it satisfies all the physical properties.

This procedure is not new for the problems considered in this report, and there has been a significant amount of literature dedicated to this problem during the last 20 years. The reason for this is that the identification problem can be posed either in the time or in the frequency domain depending on whether (9) or (10) are used in the step (i) above. This is illustrated in Table 1. In either case, different estimators (algorithms) can be applied. In general, the identification is applied to the different entries of the multiple degree-of-freedom model  $i, k = 1, \dots, 6$ .

Table 1: Identification Methods: type of data used to identify the models, and models obtained.

Data	Model Obtained
Time Domain: $K_{ik}(t)$	$\begin{bmatrix} \hat{\mathbf{A}}_{ik} & \hat{\mathbf{B}}_{ik} \\ \hat{\mathbf{C}}_{ik} & \hat{\mathbf{D}}_{ik} \end{bmatrix}$
Frequency Domain: $K_{ik}(j\omega)$	$\hat{K}_{ik}(s) = \frac{P_{ik}(s)}{Q_{ik}(s)} \Leftrightarrow \begin{bmatrix} \hat{\mathbf{A}}_{ik} & \hat{\mathbf{B}}_{ik} \\ \hat{\mathbf{C}}_{ik} & \hat{\mathbf{D}}_{ik} \end{bmatrix}$

The frequency-domain identification seeks rational transfer function approximations:

$$\hat{K}_{ik}(s) = \frac{P_{ik}(s)}{Q_{ik}(s)} = \frac{p_r s^r + p_{r-1} s^{r-1} + \dots + p_0}{s^n + q_{n-1} s^{n-1} + \dots + q_0}. \quad (12)$$

By restricting  $s$  to take only imaginary values,  $s = j\omega$ , we obtain the frequency response of the model. The coefficients of (12) are determined such this frequency response approximates the one given by (10). Once the coefficients of the transfer functions are obtained, a state space realisation can be obtained using any of the standard canonical forms—see, for example, Kailath (1980).

One property of the model that is of paramount importance is the relative degree of the transfer function (12):

$$\text{Rel deg}(\hat{K}) \triangleq \text{deg}(Q) - \text{deg}(P). \quad (13)$$

As we will see in the next section, all the transfer functions approximating fluid-memory models must have relative degree equal to one. This means that there is no static relationship in the mapping  $\dot{\xi} \mapsto \mu$ . Therefore, the matrix  $\hat{D}$  in the state-space formulation (11) must be zero.

## 5 Constraints on Parametric Approximations

An important aspect of any identification problem is the amount of *a priori* information available about the dynamic system under study and how this information is used in the identification method to set constraints on the model structure and parameters. Table 2 shows on the left-hand side column five properties of the fluid memory models—which are discussed in detail in the Appendix. These properties can be used to set constraints on the structure and parameters of the approximating model (12). Indeed, the right-hand side column of Table 2 summarises implications the properties have on the parametric model approximations.

Table 2: Properties of Retardation Functions and Implications on Parametric Approximations.

Property	Implication on Parametric Models
1) $\lim_{\omega \rightarrow 0} \mathbf{K}(j\omega) = \mathbf{0}$	There are zeros at $s = 0$ .
2) $\lim_{\omega \rightarrow \infty} \mathbf{K}(j\omega) = \mathbf{0}$	Strictly proper.
3) $\lim_{t \rightarrow 0^+} \mathbf{K}(t) \neq \mathbf{0}$	Relative degree 1.
4) $\lim_{t \rightarrow \infty} \mathbf{K}(t) = \mathbf{0}$	BIBO stable.
5) The mapping $\dot{\xi} \mapsto \mu$ is Passive	$\mathbf{K}(j\omega)$ is positive real.

The low-frequency asymptotic value (property 1 in Table 2), establishes that the transfer functions  $\hat{K}_{ik}(s)$  in (12) have a zero at  $s = 0$ . This can be used to set the constraint  $b_0 = 0$  in (12):

$$\hat{K}_{ik}(s) = \frac{P_{ik}(s)}{Q_{ik}(s)} = \frac{p_r s^r + p_{r-1} s^{r-1} + \dots + p_1 s}{s^n + q_{n-1} s^{n-1} + \dots + q_0}. \quad (14)$$

The high-frequency asymptotic value (property 2 in Table 2) establishes that the transfer function models are strictly proper, that is  $\text{deg}(Q_{ik}) > \text{deg}(P_{ik})$  since this results in the denominator growing faster than the numerator as the frequency increases, and hence, the frequency response tends asymptotically to zero. The initial-time value (property 3 in Table 2), however, imposes a further constraint on the relative degree. This property establishes that the relative degree of  $\hat{K}_{ik}(s)$  is exactly 1. Indeed, for the entries  $K_{ik}(j\omega)$ , which are not uniformly zero due to symmetry of the hull, the initial-value theorem of the Laplace transform establishes that

$$\lim_{t \rightarrow 0^+} \hat{K}_{ik}(t) = \lim_{s \rightarrow \infty} s \hat{K}_{ik}(s) = \lim_{s \rightarrow \infty} s \frac{P_{ik}(s)}{Q_{ik}(s)} = \frac{s^{r+1} p_r}{s^n}. \quad (15)$$

From (15), it follows that the limit is different from zero only if  $n = r + 1$ . Hence, the relative degree of the approximations must be 1, that is  $\text{deg}(Q_{ik}) - \text{deg}(P_{ik}) = 1$ .

The final-time value (property 4 in Table 2) establishes that the impulse response tends to zero



as time goes to infinity. This is a necessary and sufficient condition of bounded-input bounded-output stability of the models.

With regards to the property 5 in Table 2, the negative feedback interconnection of passive systems is passive; and thus, stable under observability conditions (Khalil, 2000)—further details about passivity are given in the Appendix. Figure 1 shows a block diagram representation of the Cummins Equation in the frequency domain in terms of the parametric model  $\hat{\mathbf{K}}(s)$  and the transfer function matrix  $\tilde{\mathbf{G}}(s)$ :

$$\tilde{\mathbf{G}}(s) = (s^2\mathbf{I} + [\mathbf{M} + \mathbf{A}_\infty]^{-1}\mathbf{G})^{-1}[\mathbf{M} + \mathbf{A}_\infty]^{-1}s. \quad (16)$$

The transfer function matrix  $\tilde{\mathbf{G}}(s)$  is passive (Kristiansen et al., 2005). Therefore, the interconnection shown in Figure 1 will also be passive provided the model  $\hat{\mathbf{K}}(s)$  is passive. Here lies the importance of passivity of the identified parametric model. The non-passivity of  $\hat{\mathbf{K}}(s)$  does not necessarily imply that the interconnection shown Figure 1 in will be unstable. However, since the passivity property follows from the hydrodynamics it is desirable to retain this property in the approximating model.

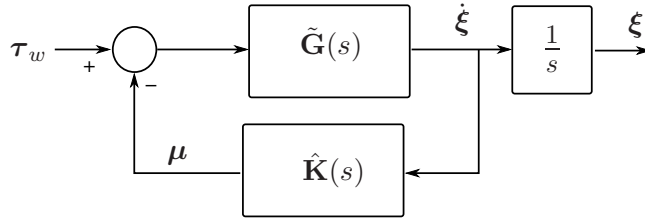


Figure 1: Block diagram of the the Cummins Equation in terms of parametric transfer functions.

## 6 Assessing the Quality of the Model

Once the parametric model for the convolution terms are obtained, we need assess how good the impulse and the frequency response are fitted. However, it is also important to check how the added mass and damping are fitted from the real and imaginary part of the parametric convolution representation (12). That is,

$$\hat{\mathbf{A}}(\omega) = \text{Im}\{\omega^{-1}\hat{\mathbf{K}}(j\omega)\} + \mathbf{A}_\infty, \quad (17)$$

$$\hat{\mathbf{B}}(\omega) = \text{Re}\{\hat{\mathbf{K}}(j\omega)\}, \quad (18)$$

where  $\text{Re}\{\cdot\}$  and  $\text{Im}\{\cdot\}$  denote the real and imaginary part.

In addition to this, one could also check how good the parametric models are with respect to the force-to-displacement frequency response

$$H_{f2d}(j\omega) = [-\omega^2[\mathbf{M} + \mathbf{A}(\omega)] + j\omega\mathbf{B}(\omega) + \mathbf{G}]^{-1}. \quad (19)$$

Indeed, using the parametric models of the convolution terms (12) we can obtain the transfer function matrix

$$\hat{\mathbf{K}}(s) = \begin{bmatrix} \frac{P_{11}(s)}{Q_{11}(s)} & \cdots & \frac{P_{16}(s)}{Q_{16}(s)} \\ \vdots & \ddots & \vdots \\ \frac{P_{61}(s)}{Q_{61}(s)} & \cdots & \frac{P_{66}(s)}{Q_{66}(s)} \end{bmatrix}. \quad (20)$$

Then, it also follows from the Laplace Transform of (4) that the force-to-displacement and force-to-velocities transfer functions are

$$\hat{\mathbf{H}}_{f2d}(s) = s^{-1}[\mathbf{I} + \tilde{\mathbf{G}}(s)\hat{\mathbf{K}}(s)]^{-1}\hat{\mathbf{K}}(s), \quad (21)$$

$$\hat{\mathbf{H}}_{f2v}(s) = [\mathbf{I} + \tilde{\mathbf{G}}(s)\hat{\mathbf{K}}(s)]^{-1}\hat{\mathbf{K}}(s), \quad (22)$$

where

$$\tilde{\mathbf{G}}(s) = (s^2\mathbf{I} + [\mathbf{M} + \mathbf{A}_\infty]^{-1}\mathbf{G})^{-1}[\mathbf{M} + \mathbf{A}_\infty]^{-1}s. \quad (23)$$

We can then compare the parametric force-to-displacement frequency response given by (21) for  $s = j\omega$  with the non-parametric frequency response given by (19).

## 7 Some Aspects of Time-domain Identification of Fluid Memory Functions

Even though this report focuses on frequency-domain identification, a few aspects of time-domain identification should be mentioned. Time-domain identification of fluid-memory models of marine structures consists of obtaining a parametric model from data of the impulse response. These methods have been proposed for example in Yu and Falnes (1995, 1998); Kristansen and Egeland (2003); Kristiansen et al. (2005).

A disadvantage of time-domain identification is that the constraints on the parameters and model structure discussed in Section 5 are not easy to enforce with time-domain identification methods. A further disadvantage is that the starting point of these methods is usually a distorted version of the true impulse response  $\mathbf{K}(t)$ . Indeed, the impulse response function computed from the frequency-domain data using (9). The integral (9) can only be computed up to finite upper frequency  $\Omega$ :

$$\mathbf{K}(t) \approx \bar{\mathbf{K}}(t) = \frac{2}{\pi} \int_0^\Omega \mathbf{B}(\omega) \cos(\omega t) d\omega. \quad (24)$$

This limitation is due to the hydrodynamic codes. In 3D or panel method codes, the size of the panels used to discretize the surface of the hull limit the accuracy of the computations at high frequency as discussed in Section 3.

The finite upper limit in the integral (24) introduces an error or distortion for all times  $t$ . The response (24) can be expressed as

$$\bar{\mathbf{K}}(t) = \frac{2}{\pi} \int_0^\infty \mathbf{W}(\omega) \mathbf{B}(\omega) \cos(\omega t) d\omega, \quad (25)$$

where  $\mathbf{W}(\omega)$  is rectangular window function, with entries defined by

$$W_{ik}(\omega) = \begin{cases} 1 & \text{if } \omega \leq \Omega, \\ 0 & \text{if } \omega > \Omega. \end{cases} \quad (26)$$

Then from the convolution property of the Fourier transform, it follows that

$$\bar{\mathbf{K}}(t) = \int_0^\infty \mathbf{W}(t - t') \mathbf{K}(t) dt', \quad (27)$$

where  $\mathbf{W}(t)$  is the inverse Fourier transform of  $\mathbf{W}(\omega)$ , which has entries

$$W_{ik}(t) = 2\Omega \frac{\sin(\Omega t)}{\Omega t}. \quad (28)$$

That is, the impulse response computed from (24) is the convolution of the true impulse response and the inverse Fourier transform of the ideal low pass filter with cut off frequency  $\Omega$ . This introduces a distortion that affects the determination of the order of the parametric approximation, and also the value of the estimated parameters. To reduce the distortion, one could use asymptotic values of  $\mathbf{B}(\omega)$  to increase  $\Omega$ . For the case of zero speed case, the following asymptotic approximations can be used (Greenhow, 1986; Perez and Fossen, 2008a):

$$\text{as } \omega \rightarrow \infty, \quad B_{ik}(\omega) \rightarrow \frac{\beta_1}{\omega^4} + \frac{\beta_2}{\omega^2}. \quad (29)$$

The use of this asymptotic values allows one to increase  $\Omega$ . Figure 2 shows the potential damping and the retardation function computed using (24). This data correspond to the pitch-pitch coupling term of a modern containership vessel presented in Perez and Fossen (2008a). The solid lines correspond to the data computed using a hydrodynamic code, whereas the dashed lines show the results corresponding to extending the damping with an asymptotic tail proportional to  $\omega^{-2}$ . The figure also shows the corresponding impulse responses computed with the original and extended data. The effect of distortion due to the finite frequency  $\Omega$  can be appreciated. Examples contrasting the quality of the models obtained via application of time- vs frequency-domain methods can be found in Perez and Fossen (2008c).

## 8 Frequency-domain Identification of Fluid-memory Models

Since the hydrodynamic codes provide hydrodynamic data as a function of the frequency, it natural to consider the identification problem *ab initio* in the frequency domain. Furthermore, the frequency-domain methods allow one to incorporate constraints on the model structure and parameters discussed in Section 5. These constraints are not easy to impose in time-domain identification methods.

In this section, we concentrate on complex curve fitting of the frequency response of the fluid memory models as a means to obtain the parameters of the approximating models. Expression (10) provides a way to compute the frequency response function  $\mathbf{K}(j\omega)$  for a finite set of frequencies. These data is the basis for the frequency-domain identification methods that seek a transfer function approximation to each entry of  $\mathbf{K}(j\omega)$ .

### 8.1 Complex Curve Fitting Revisited

Consider the non-parametric data  $\mathbf{K}(j\omega_l)$  computed for a finite set of frequencies  $l = 1, \dots, N$ . By adopting an appropriate order and relative degree for the parametric model (12) (these issues that are addressed in Section 8.3), the parameter estimation problem can be posed a complex LS curve fitting:

$$\boldsymbol{\theta}^* = \arg \min_{\boldsymbol{\theta}} \sum_l w_l \boldsymbol{\epsilon}_l^* \boldsymbol{\epsilon}_l, \quad (30)$$

where the notation  $*$  indicates transpose complex conjugate, and

$$\boldsymbol{\epsilon}_l = K_{ik}(j\omega_l) - \frac{P_{ik}(j\omega_l, \boldsymbol{\theta})}{Q_{ik}(j\omega_l, \boldsymbol{\theta})}. \quad (31)$$

and the vector of parameters  $\boldsymbol{\theta}$  is defined as

$$\boldsymbol{\theta} = [p_r, \dots, p_0, q_{n-1}, \dots, q_0]^T. \quad (32)$$

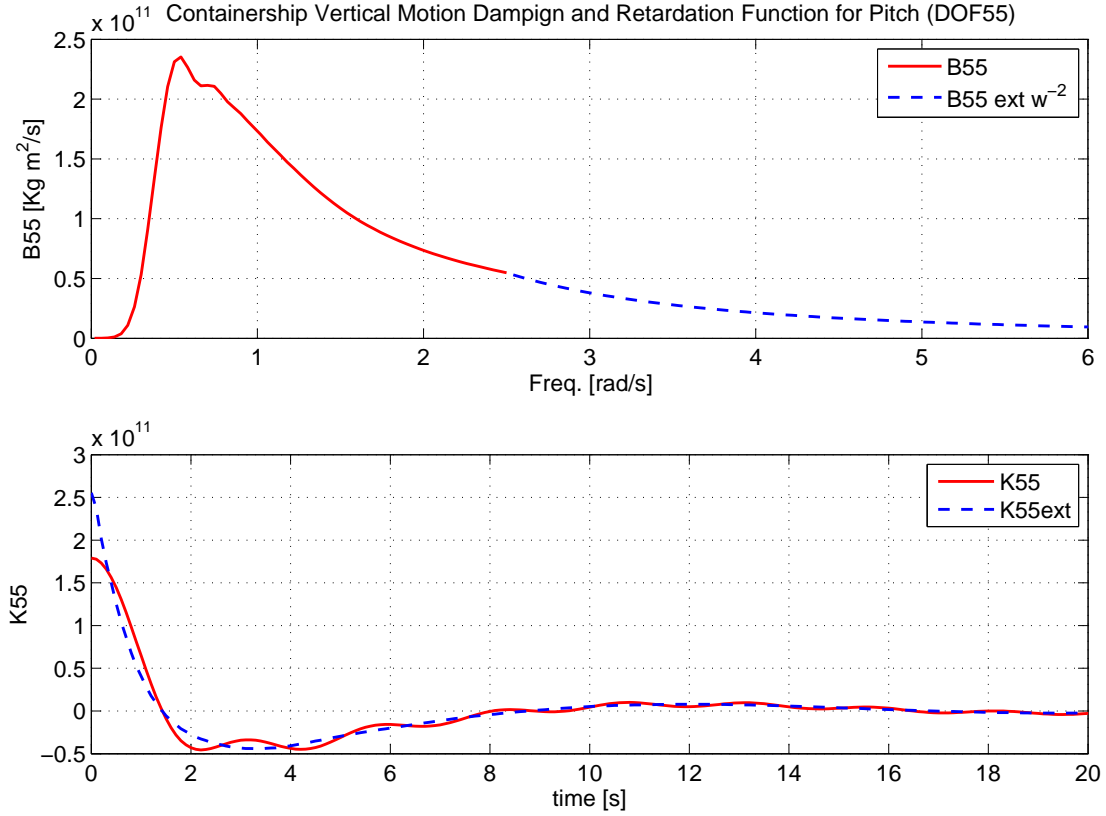


Figure 2: Potential damping and retardation function corresponding to the pitch-pitch coupling term of a modern containership vessel presented in Perez and Fossen (2008a). Solid line based on the data computed up to frequency of 2.5rad/s. Dashed line based computed data and asymptotic extension up to a frequency of 6rad/s.

The weights  $w_l$  can be exploited to select how important is the fit at different frequency ranges. The above parameter estimation problem is a non-linear LS problem in the parameters, which can be solved using a Gauss-Newton algorithm, or it can be linearized as indicated in the next section.

## 8.2 A Linearised Iterative Solution for Complex Curve Fitting

Levy (1959), proposed a linearisation of (30). That is,

$$\theta'^* = \arg \min_{\theta} \sum_l w'_l (\epsilon'_l)^* \epsilon'_l, \quad (33)$$

where

$$\epsilon'_l = Q_{ik}(j\omega_l, \theta) \tilde{K}_{ik}(j\omega_l) - P_{ik}(j\omega_l, \theta). \quad (34)$$

This problem is linear in the parameters, and thus easy to solve. Indeed, using a matrix form we can write

$$\theta'^* = \arg \min_{\theta} \epsilon'^* \mathbf{W} \epsilon', \quad (35)$$

with

$$\boldsymbol{\epsilon}' = [\epsilon'_1, \dots, \epsilon'_N]^T, \quad \mathbf{W} = \text{diag}(w'_1, w'_2, \dots, w'_n). \quad (36)$$

Using this notation, we can write

$$\boldsymbol{\epsilon}' = \boldsymbol{\Gamma} - \boldsymbol{\Phi}\boldsymbol{\theta}, \quad (37)$$

with the obvious definition for the matrices  $\boldsymbol{\Phi}$  and  $\boldsymbol{\Gamma}$ .

The solution to (35)-(37) is then given by

$$\boldsymbol{\theta}^* = (\boldsymbol{\Phi}^T \mathbf{W} \boldsymbol{\Phi})^{-1} \boldsymbol{\Phi}^T \mathbf{W} \boldsymbol{\Gamma}. \quad (38)$$

The linearised problem (33) derives from the non-linear problem (30) by choosing

$$w_l = w'_l |Q(j\omega_l, \boldsymbol{\theta})|^2. \quad (39)$$

This means that solving (33) can be thought as solving (30) with the weights as given in (39). A problem with this linear formulation is that the identified transfer function does not in general give a good fitting. For example, when the data extends over a large range of frequencies or when  $Q(s)$  has poorly damped complex roots close to the imaginary axis, the coefficients  $w_l$  in (39) will weight the fitting more heavily at high frequencies and less heavily at low frequencies and those close to the resonant roots. This weighting normally gives a bias in the parameter estimates.

Sanathanan and Koerner (1963) proposed a method to compensate for the bias introduced by the linearisation. This method consists in solving (35)-(37) iteratively using as weighting coefficients the inverse of the denominator  $Q(j\omega, \boldsymbol{\theta})$  evaluated at the previous estimate. This algorithm can be summarised in the following:

1. Set  $\mathbf{W}_0 = \mathbf{I}$ .
2. Solve  $\boldsymbol{\theta}_n^* = \arg \min_{\boldsymbol{\theta}} \boldsymbol{\epsilon}'^* \mathbf{W}_n \boldsymbol{\epsilon}'$ ,
3. Set  $\mathbf{W}_{n+1} = \text{diag}(|Q_{ik}(j\omega_l, \boldsymbol{\theta}_n)|^{-2})$  go to 2 until convergence.

This choice of weighting coefficients in step 3 results in the following problem at each step  $n$  of the iteration:

$$\boldsymbol{\theta}_n^* = \arg \min_{\boldsymbol{\theta}} \sum_l \left| \frac{Q_{ik}(j\omega_l, \boldsymbol{\theta}) K_{ik}(j\omega_l)}{Q_{ik}(j\omega_l, \boldsymbol{\theta}_{n-1}^*)} - \frac{P_{ik}(j\omega_l, \boldsymbol{\theta})}{Q_{ik}(j\omega_l, \boldsymbol{\theta}_{n-1}^*)} \right|^2, \quad (40)$$

For data with low level of noise convergence is reached after a few iterations (10 to 20),  $\boldsymbol{\theta}_n^* \approx \boldsymbol{\theta}_{n-1}^*$ ; and thus, the original non-linear LS problem (30) is approximately recovered (Unbehauen and Rao, 1987).

## 8.3 Practical Issues Associated with the Identification of Fluid-memory Approximations

### 8.3.1 Preparing the Data

Since the retardation functions relate the velocities to the radiation forces, the numerator coefficients in (12) can take large values compared to those of the denominator. This can result in a numerically ill-conditioned problem (40).

To avoid numerical problems, it is convenient to scale the data before performing the identification:

$$K'_{ik}(j\omega) = \alpha K_{ik}(j\omega), \quad (41)$$

with

$$\alpha \triangleq \frac{1}{\max |K_{ik}(j\omega)|}. \quad (42)$$

That is, one should fit a rational transfer function to  $K'_{ik}(j\omega)$  and then multiply the resulting numerator by  $\alpha^{-1}$  to obtain our estimate of  $K_{ik}(j\omega)$ .

The accuracy of the data has obviously a significant bearing on the identification. Thus, whenever the data at a range of frequencies is believed to be inaccurate, it should not be used for identification. It is also important to eliminate wild points. These irregularities in the data can be inspected visually from the plots of added mass  $A_{ik}(j\omega)$  and potential damping  $B_{ik}(j\omega)$  of each entry.

### 8.3.2 Adding Prior Knowledge

Based on the information provided in Table 2, it follows that the rational transfer functions (12) have

- A zero at  $s=0$ ,
- Relative degree 1; i.e.,  $r = n - 1$  where  $n = \deg(Q)$ , and  $r = \deg(P)$ .

The constraint that the functions have a zero at  $s = 0$ , can be addressed by “integrating” the data in the frequency domain. Indeed, we can factorise

$$P_{ik}(s) = s P'_{ik}(s), \quad (43)$$

where  $P'_{ik}(s)$  does not have roots on the imaginary axis of the complex plane and has degree  $\deg(P'_{ik}) = n - 2$ . Then, we can express (12) as follows,

$$\hat{K}_{ik}(j\omega) = \frac{(j\omega)P'_{ik}(j\omega, \boldsymbol{\theta}_{ik})}{Q_{ik}(j\omega, \boldsymbol{\theta}_{ik})}. \quad (44)$$

We can further divide (44) by  $j\omega$ , which is the equivalent of integrating the data in the time domain,

$$\frac{\hat{K}_{ik}(j\omega)}{(j\omega)} = \frac{P'_{ik}(j\omega, \boldsymbol{\theta}_{ik})}{Q_{ik}(j\omega, \boldsymbol{\theta}_{ik})}, \quad (45)$$

and then fit

$$\boldsymbol{\theta}_{ik}^* = \arg \min_{\boldsymbol{\theta}} \sum_l \left| \frac{K_{ik}(j\omega_l)}{(j\omega_l)} - \frac{P'_{ik}(j\omega_l, \boldsymbol{\theta})}{Q_{ik}(j\omega_l, \boldsymbol{\theta})} \right|^2. \quad (46)$$

Since the LS method discussed in Sections 8.1 and 8.2 was introduced for a general case, this simply implies that we need to choose only the order  $n$  to apply the method with  $r = n - 2$ . Then after  $P'_{ik}(s)$  is identified, the factor  $s$  can be incorporated to the numerator polynomial to form  $P_{ik}(s)$  according to (43).

### 8.3.3 Oder selection

The order of the transfer functions depends on the hydrodynamic characteristics of the vessel or marine structure; i.e., it depends on the hull shape. Based on the properties of the convolution terms given in Table 2, it follows that the minimum order transfer function that satisfies all the properties is a second order one:

$$\hat{K}_{ik}^{min}(s) = \frac{p_0 s}{s^2 + q_1 s + q_0}.$$

Therefore, one can start with this minimum order transfer function ( $n=2$ ), and increase the order while monitoring that the LS cost decreases—or simply by visual inspection of the fitted frequency response and the added mass and damping computed from the approximation as indicated in (17) and (18). If the order of the proposed model is too large, there will be over-fitting and therefore, the cost will increase; however before this happens, the value of the cost normally remains unchanged as one increments the order of the system.

### 8.3.4 Stability

The resulting model from the LS minimization may not necessarily be stable because stability is not enforced as a constraint in the optimisation. This can be addressed after the identification. Should the obtained model be unstable, one could obtain a stable one by reflecting the unstable poles about the imaginary axis and re-computing the denominator polynomial. That is,

- (i) Compute the roots of  $\lambda_1, \dots, \lambda_n$  of  $Q_{ik}(s, \hat{\theta}_{ik})$ .
- (ii) If  $\text{Re}\{\lambda_i\} > 0$ , then set  $\text{Re}\{\lambda_i\} = -\text{Re}\{\lambda_i\}$ ,
- (iii) Reconstruct the polynomial:  $Q_{ik}(s) = (s - \lambda_1)(s - \lambda_1) \cdots (s - \lambda_n)$ .

When the validity of the model is assessed, this should be done with a stable model.

### 8.3.5 Passivity

A disadvantage of the method of LS curve fitting is that it does not enforce passivity. If passivity is required (i.e.,  $B_{ik}(\omega) > 0$ ), a simple way to ensure it is to try different order approximations and choose the one that is passive. The approximation is passive if

$$\text{Re} \left\{ \frac{P_{ik}(j\omega_l, \boldsymbol{\theta})}{Q_{ik}(j\omega_l, \boldsymbol{\theta})} \right\} > 0. \quad (47)$$

When this is checked, one should evaluate the transfer function at low and high frequencies—below and above the frequencies used for the parameter estimation.

Often, low-order approximations models of the convolution terms given by this method are passive—the term ‘low’ depends on the data of the particular vessel under consideration. Therefore, one can reduce the order and trade-off fitting accuracy for passivity. A different approach would be optimise the numerator of the obtained non passive model to obtain a passive approximation—this goes beyond the scope of this paper, but the reader is referred to Damaren (2000) and references therein.

## 8.4 A practical Algorithm for the Identification Fluid-memory Models

To summarise the identification process based on LS-fitting of the frequency response of the retardation functions, taking into consideration all the issues discussed in the previous section, we present the following algorithm:

1. Set the appropriate range of frequencies where the hydrodynamic data is considered accurate, eliminate wild points, and compute the frequency response for a set of frequencies  $\omega_l$ :

$$K_{ik}(j\omega_l) = B_{ik}(\omega_l) - j\omega(A_{ik}(\omega_l) - A_{\infty,ik}). \quad (48)$$

2. Scale the data:

$$K'_{ik}(j\omega_l) = \alpha K_{ik}(j\omega_l), \quad \alpha \triangleq \frac{1}{\max |K_{ik}(j\omega_l)|}. \quad (49)$$

3. Select the order of the approximation  $n = \deg(Q_{ik}(j\omega, \boldsymbol{\theta}_{ik}))$ . The minimum order approximation  $n=2$  can be the starting point.

4. Estimate the parameters

$$\boldsymbol{\theta}_{ik}^* = \arg \min_{\boldsymbol{\theta}} \sum_l \left| \frac{K'_{ik}(j\omega_l)}{(j\omega_l)} - \frac{P'_{ik}(j\omega_l, \boldsymbol{\theta})}{Q_{ik}(j\omega_l, \boldsymbol{\theta})} \right|^2, \quad (50)$$

with  $\deg(P'_{ik}(j\omega, \boldsymbol{\theta}_{ik})) = n - 2$ . Use the iterative linear LS solution described in Section 8.2.

5. Check stability by computing the roots of  $Q_{ik}(j\omega, \boldsymbol{\theta}_{ik}^*)$  and change the real part of those roots with positive real part—see Section 8.3.
6. Construct the desired transfer function by scaling and incorporate the  $s$  factor in the numerator:

$$\hat{K}_{ik}(s) = \frac{1}{\alpha} \frac{s P'_{ik}(s, \boldsymbol{\theta}_{ik}^*)}{Q_{ik}(s, \boldsymbol{\theta}_{ik}^*)}. \quad (51)$$

7. Estimate the added-mass and damping based on the identified parametric approximation via

$$\hat{A}_{ik}(\omega) = \text{Im}\{\omega^{-1} \hat{K}_{ik}(j\omega)\} + A_{\infty,ik} \quad (52)$$

$$\hat{B}_{ik}(\omega) = \text{Re}\{\hat{K}_{ik}(j\omega)\}, \quad (53)$$

and compare with the  $A_{ik}(\omega)$  and  $B_{ik}(\omega)$  given by the hydrodynamic code. If the fitting is not satisfactory increase the order of the approximation and go back to step (iii).

8. Check for passivity if required  $\hat{B}_{ik}(j\omega) > 0$ .



## 9 Joint Identification of Infinite-frequency Added Mass and Fluid Memory Models

As discussed in Section 3, hydrodynamic codes based on 2D potential theory do not normally provide the value of the infinite frequency added mass coefficient  $\mathbf{A}_\infty = \lim_{\omega \rightarrow \infty} \mathbf{A}(\omega)$ . In these cases, we cannot form  $\mathbf{K}(j\omega)$  as indicated in (10).

Kaasen and Mo (2004) addressed this problem by making a partial-fraction expansion of the real part of  $\hat{K}_{ik}(s)$  in terms of  $\omega^2$ . The poles and residuals of this expansion can be estimated using LS fitting to the damping data  $B_{ik}(\omega)$ . Then  $\hat{K}_{ik}(s)$  can be obtained by mapping poles and the residuals of the partial-fraction expansion of its real part into the poles and residuals of a partial fraction expansion of  $\hat{K}_{ik}(s)$  in terms  $j\omega$ . This method is rather complicated and the mapping from one set of residuals to the other requires careful consideration.

In this section, present a simpler alternative to the method of Kaasen and Mo (2004) proposed in Perez and Fossen (2008b). The proposed method exploits the knowledge and methods used in the identification of  $\hat{K}_{ik}(s)$  discussed in the Section 8, and therefore, it provides a natural extension of those results putting the two identification problems into the same framework.

The frequency-domain representation of the radiation forces given in (5) can be alternatively expressed as

$$\tau_{rad,ik}(j\omega) = \left[ \frac{B_{ik}(\omega)}{j\omega} + A_{ik}(\omega) \right] \ddot{\xi}(s), \quad (54)$$

where the expression in brackets gives the complex coefficient

$$\tilde{A}(j\omega) \triangleq \frac{B_{ik}(\omega)}{j\omega} + A_{ik}(\omega). \quad (55)$$

From the Laplace transform of (3), and a rational approximation for the convolution term, it also follows that

$$\hat{\tau}_{rad,ik}(s) = \left[ A_{\infty,ik} s + \frac{P_{ik}(s)}{Q_{ik}(s)} \right] \dot{\xi}(s), \quad (56)$$

$$= \left[ A_{\infty,ik} + \frac{P'_{ik}(s)}{Q_{ik}(s)} \right] \ddot{\xi}(s), \quad (57)$$

with  $P_{ik}(s) = s P'_{ik}(s)$ . This representation can be traced back to the work of Söding (1982), and it has been used by Xia et al. (1998) and Sutulo and Guedes-Soares (2005), but with a different approach to that presented in this paper.

The transfer function in brackets in (57) can be further expresses as

$$\hat{A}_{ik}(s) = \frac{R_{ik}(s)}{S_{ik}(s)} = \frac{A_{\infty,ik} Q_{ik}(s) + P'_{ik}(s)}{Q_{ik}(s)}, \quad (58)$$

from which it follows that  $\deg(R_{ik}) = \deg(S_{ik}) = n$ . Therefore, we can follow the same approach as in Section 8 and use LS optimisation to estimate the parameters of the polynomial  $R_{ik}$  and  $S_{ik}$  given the frequency-respose data (55):

$$\boldsymbol{\theta}^* = \arg \min_{\boldsymbol{\theta}} \sum_l w_l (\epsilon_l^* \epsilon_l), \quad (59)$$

with

$$\epsilon_l = \tilde{A}_{ik}(j\omega_l) - \frac{R_{ik}(j\omega_l, \boldsymbol{\theta})}{S_{ik}(j\omega_l, \boldsymbol{\theta})}, \quad (60)$$

with the constraint that  $n = \deg S_{ik}(s) = \deg R_{ik}(s)$ . We also know from Section 8.3 that the minimum order approximation is of  $n = 2$ . Therefore, we can start with this order and increment to improve the fit if necessary.

It should be noted as well that if we normalised the polynomial  $S_{ik}(s)$  to be monic as  $Q_{ik}(s)$  is in (12), then

$$\hat{A}_{\infty,ik} = \lim_{\omega \rightarrow \infty} \frac{R_{ik}(s, \boldsymbol{\theta}^*)}{S_{ik}(s, \boldsymbol{\theta}^*)}, \quad (61)$$

that is, the infinite-frequency added mass  $\hat{A}_{\infty,ik}$  is the coefficient of the highest order term of  $R_{ik}(s, \boldsymbol{\theta}^*)$ .

Therefore, after obtaining  $R_{ik}(s, \boldsymbol{\theta}^*)$  and  $S_{ik}(s, \boldsymbol{\theta}^*)$ , we can recover the polynomials for the fluid-memory model together with the infinite added mass coefficients:

$$\begin{aligned} Q_{ik}(s, \boldsymbol{\theta}^*) &= S_{ik}(s, \boldsymbol{\theta}^*), \\ P_{ik}(s, \boldsymbol{\theta}^*) &= R_{ik}(s, \boldsymbol{\theta}^*) - \hat{A}_{\infty,ik} S_{ik}(s, \boldsymbol{\theta}^*). \end{aligned} \quad (62)$$

In the next section, we provide different application examples to illustrate the use of the identification methods proposed.

## 10 Application Examples

In this section, we consider two application examples. The first example is a semi-submersible, and the identification is based on 3D data. The second example is a FPSO, and the identification is done without using the data of the infinite frequency added mass.

### 10.1 Identification of Fluid-memory models of a Semi-submersible.

An offshore structure like a semi-submersible provides an interesting example with challenging frequency response fittings to assess the applicability of the method and the use of constraints discussed in this paper. Figure 3 shows the bow half-hull of a semi-submersible used to compute hydrodynamic data with the 3D code WAMIT. These data are part of a demo of the Marine Systems Simulator available at [www.marinecontrol.org](http://www.marinecontrol.org). Figures 4 to 7 show the results of frequency domain identification incorporating constraints for all the couplings. Since the structure has fore-aft and port-starboard symmetry, the only cross-coupling term is 2-4, with results shown in Figure 5. Note that all diagonal terms are passive, except for the cross-coupling term, which for this example does not require a passive approximation. These figures show very good results for complex fittings with parametric models of orders between 5 and 8.

### 10.2 Identification of the Joint Infinite-frequency Added Mass and Fluid-memory models of a FPSO.

In order to illustrate the method for joint identification of infinite added mass and damping, we will consider the data of a FPSO corresponding to the vertical plane motion. Figure 8 shows the hull geometry for the vessel. We will use 3D-data to evaluate the accuracy of the method. That is, the

value of the true  $A_{\infty,ik}$  and  $K_{ik}(j\omega)$  are known, but the identification is done only in terms of  $A_{ik}(\omega)$  and  $B_{ik}(\omega)$  forming the complex coefficient  $\tilde{A}_{ik}(j\omega)$  according to (55).

Figure 9 shows the data fit of the complex coefficient  $\tilde{A}_{33}(j\omega)$  based on a parametric transfer function approximation of order 4. From the plot of the phase, we can see that the model has no zeros at zero frequency and also that the relative degree is zero. These properties, evidenced in the low- and high-frequency asymptotic values of the phase, are in agreement with expression (58) and the properties of the fluid memory terms. Figure 10 shows the estimates of the infinite-frequency added mass coefficient and the corresponding fluid-memory model according to (61) and (62). Figures 11 and 12 show similar results for the couplings 5-3 and 5-5 respectively.

Table 3 shows the numerical results for the estimates of infinite-frequency added mass coefficients, and their corresponding relative errors. As we can see all the estimates are within 2% of the true values computed by the hydrodynamic code.

Table 3: True and identified infinite-frequency added mass coefficients of a FPSO for the vertical plane motion couplings.

True Value	Identified	Rel. Err.
$A_{\infty,33}=1.7283e8$	$\hat{A}_{\infty,33}= 1.731e8$	1.5 %
$A_{\infty,35}=-3.463e7$	$\hat{A}_{\infty,35}=-3.7179e7$	0.18%
$A_{\infty,55}= 3.9154e11$	$\hat{A}_{\infty,55}=3.9293e11$	0.35%

## 11 Conclusions

This report addresses the issue of using constraints on model structure and parameters to refine the search of approximating parametric models to the fluid-memory terms of the Cummins equation. These models form the basis of ship simulators and design of ship motion control systems.

Hydrodynamic properties of the fluid memory terms are analysed and their consequences on the structure and parameters of the models discussed. It is then argued that frequency-domain identification methods are more favourable than time-domain methods. The first reason for this is that the former allow direct use of the constraints. Although frequency-domain identification methods have been proposed before for this particular application, a discussion about the use of constraints has not been explicitly presented in the literature. The second reason for favouring frequency-domain methods is that having set the correct constraints on the model structure and parameters, is it not necessary to compute hydrodynamic data at either very low or very high frequency, as it is in the case of time-domain methods. This presents a significant advantage for both 3D and 2D hydrodynamic codes use to compute the data.

A new extension to the method of frequency-domain identification is presented to accommodate for 2D data obtained from strip theory codes, which do not normally estimate the infinite frequency added mass. The extended method makes use of the properties of the fluid-memory models to derive constraints on parametric approximation models of a complex coefficient that depends only on the frequency dependant added mass and damping. This parametric approximation is then obtained following the same procedures as in the case of 3D data, and from this model both the infinite-frequency

added mass and fluid-memory model are obtained. Hence, the identification problems using either 3D or 2D data can be considered within the same framework.

The quality of the models obtained with proposed identification methods are illustrated using hydrodynamic data of two different marine structures. Data in 6DOF of a semi-submersible is used to demonstrate that frequency-domain methods based on LS with the appropriate constraints are able to fit non-trivial frequency responses. Finally, data of the vertical plane motion of a FPSO was used to illustrate the performance of the identification of joint infinite-frequency added mass and fluid memory models. The proposed method yields accurate estimates.

## References

- Beck, R. and Reed, A. Modern computational methods for ships in a seaway. *SNAME Transactions*, 2001. 109:1–51.
- Cummins, W. The impulse response function and ship motion. Technical Report 1661, David Taylor Model Basin–DTNSRDC, 1962.
- Damaren, C. Time-domain floating body dynamics by rational approximations of the radiation impedance and diffraction mapping. *Ocean Engineering*, 2000. 27:687–705.
- Faltinsen, O. *Sea Loads on Ships and Offshore Structures*. Cambridge University Press, 1990.
- Greenhow, M. High- and low-frequency asymptotic consequences of the Kramers-Kronig relations. *J. Eng. Math.*, 1986. 20:293–306.
- Hjulstad, A., Kristansen, E., and Egeland, O. State-space representation of frequency-dependant hydrodynamic coefficients. In *Proc. IFAC Conference on Control Applications in Marine Systems*. 2004 .
- Holappa, K. and Falzarano, J. Application of extended state space to nonlinear ship rolling. *Ocean Engineering*, 1999. 26:227–240.
- Jefferys, E., Broome, D., and Patel, M. A transfer function method of modelling systems with frequency dependant coefficients. *Journal of Guidance Control and Dynamics*, 1984. 7(4):490–494.
- Jefferys, E. and Goheen, K. Time domain models from frequency domain descriptions: Application to marine structures. *International Journal of Offshore and Polar Engineering*, 1992. 2:191–197.
- Jordan, M. and Beltran-Aguedo, R. Optimal identification of potential-radiation hydrodynamics of moored floating stuctures. *Ocean Engineering*, 2004. 31:1859–1914.
- Kaasen, K. and Mo, K. Efficient time-domain model for frequency-dependent added mass and damping. In *23rd Conference on Offshore Mechanics and Arctic Engineering (OMAE), Vancouver, Canada*. 2004 .
- Kailath, T. *Linear systems*. Prentice Hall, 1980.
- Khalil, H. *Nonlinear Systems*. Prentice Hall, 2000.

- Kristansen, E. and Egeland, O. Frequency dependent added mass in models for controller design for wave motion ship damping. In *6th IFAC Conference on Manoeuvring and Control of Marine Craft MCMC'03, Girona, Spain*. 2003 .
- Kristiansen, E., Hjuslstad, A., and Egeland, O. State-space representation of radiation forces in time-domain vessel models. *Ocean Engineering*, 2005. 32:2195–2216.
- Levy, E. Complex curve fitting. *IRE Trans. Autom. Control*, 1959. AC-4:37–43.
- Lozano, R., Brogliato, B., Egeland, O., and Masche, B. *Dissipative Systems Analysis and Control, Theory and Applications*. Springer, 2000.
- McCabe, A., Bradshaw, A., and Widden, M. A time-domain model of a floating body using transforms. In *Proc. of 6th European Wave and Tidal energy Conference*. University of Strathclyde, Glasgow, U.K., 2005 .
- Newman, J. *Marine Hydrodynamics*. MIT Press, 1977.
- Ogilvie, T. Recent progress towards the understanding and prediction of ship motions. In *6th Symposium on Naval Hydrodynamics*. 1964 .
- Parzen, E. Some conditions for uniform convergence of integrals. *Proc. of The American mathematical Society*, 1954. 5(1):55–58.
- Perez, T. and Fossen, T. A derivation of high-frequency asymptotic values of 3D added mass and damping based on properties of the Cummins equation. *Journal of Maritime Research*, 2008a. 5(1):65–78.
- Perez, T. and Fossen, T. Joint identification of infinite-frequency added mass and fluid-memory models of marine structures. *Modeling Identification and Control, published by The Norwegian Society of Automatic Control.*, 2008b. 29(3):93102.
- Perez, T. and Fossen, T. I. Time-domain vs. frequency-domain identification of parametric radiation force models for marine structures at zero speed. *Modeling Identification and Control, published by The Norwegian Society of Automatic Control.*, 2008c. 29(1):1–19.
- Salvesen, N., Tuck, E., and Faltinsen, O. Ship motions and sea loads. *Trans. The Society of Naval Architects and Marine Engineers–SNAME*, 1970. 10:345–356.
- Sanathanan, C. and Koerner, J. Transfer function synthesis as a ratio of two complex polynomials. *IEEE Trnas. of Autom. Control*, 1963.
- Söding, H. Leckstabilität im seegang. Technical report, Report 429 of the Institut für Schiffbau, Hamburg, 1982.
- Sutulo, S. and Guedes-Soares, C. An implementation of the method of auxiliary state variables for solving seakeeping problems. *Int. Ship Buildg. Progress*, 2005. 52(4):357–384.
- Taghipour, R., Perez, T., and Moan, T. Time domain hydroelastic analysis of a flexible marine structure using state-space models. In *26th International Conference on Offshore Mechanics and Arctic Engineering-OMAE 07, San Diego, CA, USA*. 2007 .
- Taghipour, R., Perez, T., and Moan, T. Hybrid frequency–time domain models for dynamic response analysis of marine structures. *Ocean Engineering*, 2008. doi:10.1016/j.oceaneng.2007.11.002.

Unbehauen, H. and Rao, G. P. *Identification of Continuous Systems*, volume 10 of *North-Holland Systems and Control Series*. North-Holland, 1987.

Xia, J., Wang, Z., and Jensen, J. Nonlinear wave-loads and ship responses by a time-domain strip theory. *Marine structures*, 1998. 11:101–123.

Yu, Z. and Falnes, J. Spate-space modelling of a vertical cylinder in heave. *Applied Ocean Research*, 1995. 17:265–275.

Yu, Z. and Falnes, J. State-space modelling of dynamic systems in ocean engineering. *Journal of hydrodynamics*, China Ocean Press, 1998. pages 1–17.

## A Properties of the Fluid Memory Models

### A.1 Initial-Time Value

The initial-time value of the retardation function (9) is non-zero and finite:

$$\lim_{t \rightarrow 0^+} \mathbf{K}(t) = \lim_{t \rightarrow 0^+} \frac{2}{\pi} \int_0^\infty \mathbf{B}(\omega) \cos(\omega t) d\omega = \frac{2}{\pi} \int_0^\infty \mathbf{B}(\omega) d\omega \neq \mathbf{0}, \quad (63)$$

The second equality follows from the application of the Riemann-Lebesgue Lemma (Ogilvie, 1964), and the last inequality is a consequence of energy considerations, which establish that  $B_{ii}(\omega) > 0$  (Faltinsen, 1990). For the off-diagonal couplings (which are not uniformly zero due to the symmetry of the hull), the damping can be negative at some frequencies, but the area under the damping curve is generally non-zero. Note that regularity conditions are satisfied for the exchange of limit and integration (Parzen, 1954).

### A.2 Final-Time Value

The final-time asymptotic value of the retardation function (9) is zero:

$$\lim_{t \rightarrow \infty} \mathbf{K}(t) = \lim_{t \rightarrow 0^+} \frac{2}{\pi} \int_0^\infty \mathbf{B}(\omega) \cos(\omega t) d\omega = \mathbf{0}. \quad (64)$$

This statement follows from (9) and the application of the Riemann-Lebesgue Lemma (Ogilvie, 1964). This property establishes necessary and sufficient conditions for bounded-input bounded-output (BIBO) stability of the convolution term in the Cummins Equation.

### A.3 Low-frequency Asymptotic Value

The low-frequency asymptotic value of the retardation function is zero ( $\lim_{\omega \rightarrow 0} \mathbf{K}(j\omega) = \mathbf{0}$ ). This statement follows from (10). In the limit as  $\omega \rightarrow 0$ , the potential damping  $\mathbf{B}(\omega)$  tends to zero since structure cannot generate waves at zero frequency. This is because the approximating free-surface condition establishes that there cannot be both horizontal and vertical and velocity components in the free surface (Faltinsen, 1990). On the other hand, in the limit as  $\omega \rightarrow 0$  the imaginary part tends to zero since the difference  $\mathbf{A}(0) - \mathbf{A}_\infty$  is finite:

$$\mathbf{A}(0) - \mathbf{A}_\infty = \lim_{\omega \rightarrow 0} -\frac{1}{\omega} \int_0^\infty \mathbf{K}(t) \sin(\omega t) dt = \int_0^\infty \mathbf{K}(t) \lim_{\omega \rightarrow 0} \frac{-\sin(\omega t)}{\omega} dt = -\int_0^\infty \mathbf{K}(t) dt < \infty.$$

Note that regularity conditions are satisfied for the exchange of limit and integration (Parzen, 1954); *i.e.*,  $\mathbf{K}_n(t) = \mathbf{K}(t) \sin(2\pi t/n)/(2\pi t/n)$  converges uniformly to  $\mathbf{K}(t)$  as  $n \rightarrow \infty$ . The last equality follows from (64).

#### A.4 High-frequency Asymptotic Value

The high-frequency asymptotic value of the retardation function is zero ( $\lim_{\omega \rightarrow \infty} \mathbf{K}(j\omega) = \mathbf{0}$ .) This statement follows from (10). In the limit as  $\omega \rightarrow \infty$ , the real part tends to zero since there cannot be generate waves. As in the case of zero frequency, this is because the approximating free-surface condition establishes that there cannot be both horizontal and vertical and velocity components in the free surface (Faltinsen, 1990). The imaginary part also tends to zero, and this follows from (7) and the Riemann-Lebesgue Lemma (Ogilvie, 1964):

$$\lim_{\omega \rightarrow \infty} \omega[\mathbf{A}(\omega) - \mathbf{A}_\infty] = \lim_{\omega \rightarrow \infty} - \int_0^\infty \mathbf{K}(t) \sin(\omega t) dt = \mathbf{0}.$$

#### A.5 Passivity

Passivity describes an intrinsic characteristic of systems that can store and dissipate energy, but not create it. The concept of energy can be generalised, and passivity formalised in mathematical terms to be used even for non-physical systems. If a system has a vector input  $\mathbf{u}$ , vector output  $\mathbf{y}$  and some internal vector variable  $\mathbf{x}$ , which can be used to quantify the amount of energy stored in the system  $V(\mathbf{x})$ . Then the passivity property of the system establishes that the energy absorbed by the system must be greater than or equal to the energy stored in the system:

$$\int_0^t \mathbf{u}^T(t') \mathbf{y}(t') dt' \geq V(\mathbf{x}(T)) - V(\mathbf{x}(0)).$$

Since this holds for all  $t$ , the instantaneous power satisfies:  $\mathbf{u}^T(t) \mathbf{y}(t) \geq \dot{V}(\mathbf{x}(t))$ . If this is satisfied, the system is said to be *passive*. The reader should refer, for example, to Khalil (2000) for a formal discussion.

Damaren (2000) discussed the passivity of the fluid-memory models. In his approach, he considered the mechanical energy of the system (kinetic + potential):

$$V(t) = \frac{1}{2} \dot{\boldsymbol{\xi}}^T \mathbf{M} \dot{\boldsymbol{\xi}} + \frac{1}{2} \boldsymbol{\xi}^T \mathbf{C} \boldsymbol{\xi}.$$

By considering only the radiation problem (no incident waves),  $\mathbf{M} \ddot{\boldsymbol{\xi}} + \mathbf{C} \dot{\boldsymbol{\xi}} = \boldsymbol{\tau}_R$ , the time-derivative of the energy reduces to  $\dot{V} = \dot{\boldsymbol{\xi}}^T \boldsymbol{\tau}_R$ ; and thus

$$V(T) - V(0) = \int_0^T \boldsymbol{\tau}_R^T \dot{\boldsymbol{\xi}} dt'.$$

This result establishes that the mapping  $\dot{\boldsymbol{\xi}} \mapsto \boldsymbol{\tau}_R$  is passive (Lozano et al., 2000). Therefore, the convolution term in the Cummins Equation is a passive mapping. An alternative derivation to the one above can be found in Kristiansen et al. (2005).

For linear-time-invariant systems a necessary and sufficient condition for passivity can be translated into the frequency domain as positive realness; that is, the real part of the transfer function is positive for all frequencies. This implies that  $\text{Re}\{\mathbf{K}(j\omega)\} \geq 0, \quad \forall \omega$ . In the case of structures with zero-average forward speed, this follows from the fact that  $\mathbf{B}(\omega) = \mathbf{B}(\omega)^T \geq 0$ , which implies that  $B_{ii}(\omega) > 0$  for all  $\omega$  (Newman, 1977; Faltinsen, 1990). The non-diagonal terms  $K_{ik}(s), i \neq k$  do not necessarily have to be positive real.



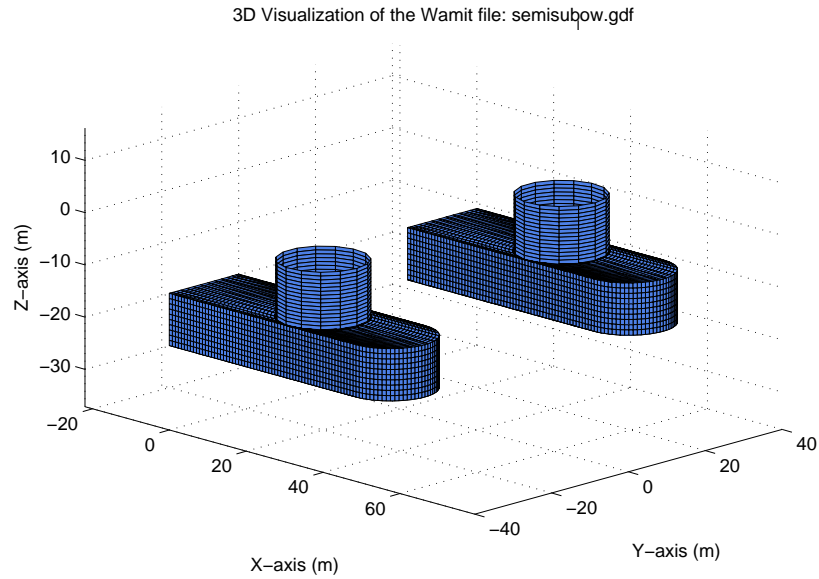


Figure 3: Hull geometry of a Semi-submersible. Data from [www.marinecontrol.org](http://www.marinecontrol.org)

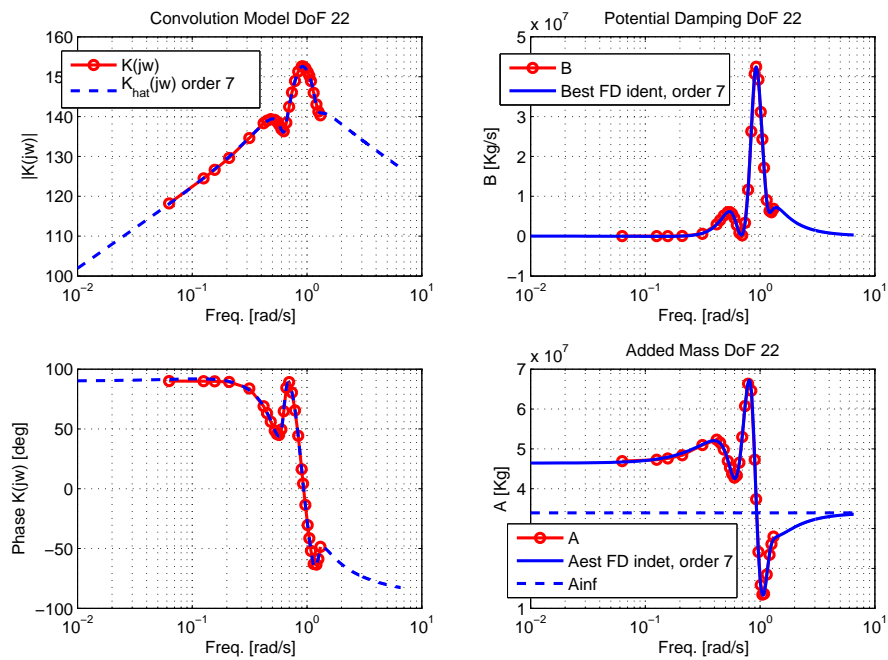


Figure 4: Data fit corresponding to the coupling 2-2 of a semi-submersible. The left hand side plots show the magnitude and phase of  $K_{22}(j\omega)$  and  $\hat{K}_{22}(j\omega)$  for a parametric approximation of order 7. The right-hand side plots show damping and added mass computed by the code and the approximations based on  $\hat{K}_{22}(j\omega)$ .



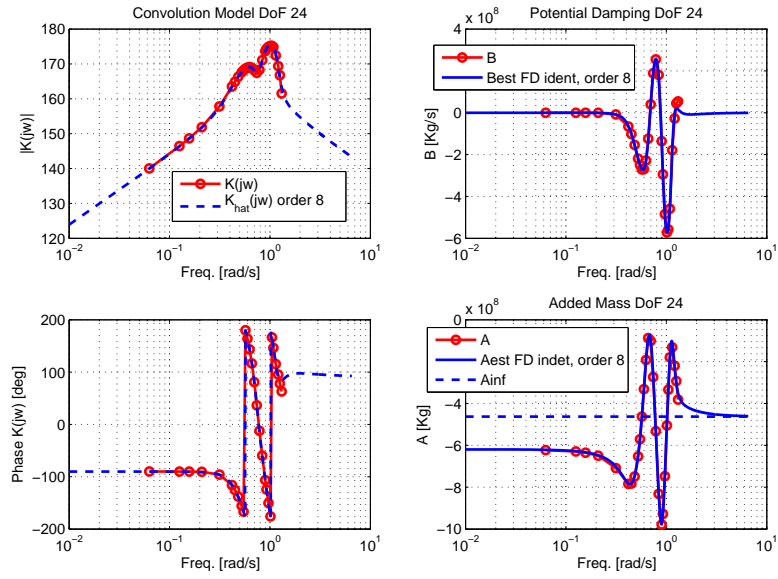


Figure 5: Data fit corresponding to the coupling 2-4 of a semi-submersible. The left hand side plots show the magnitude and phase of  $K_{24}(j\omega)$  and  $\hat{K}_{24}(j\omega)$  for a parametric approximation of order 8. The right-hand side plots show damping and added mass computed by the code and the approximations based on  $\hat{K}_{24}(j\omega)$ .

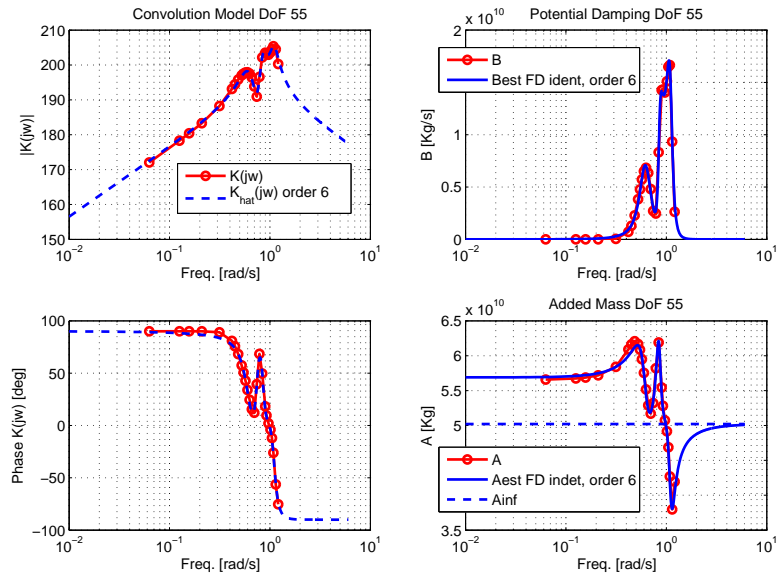


Figure 6: Data fit corresponding to the coupling 5-5 of a semi-submersible. The left hand side plots show the magnitude and phase of  $K_{55}(j\omega)$  and  $\hat{K}_{55}(j\omega)$  for a parametric approximation of order 6. The right-hand side plots show damping and added mass computed by the code and the approximations based on  $\hat{K}_{44}(j\omega)$ .

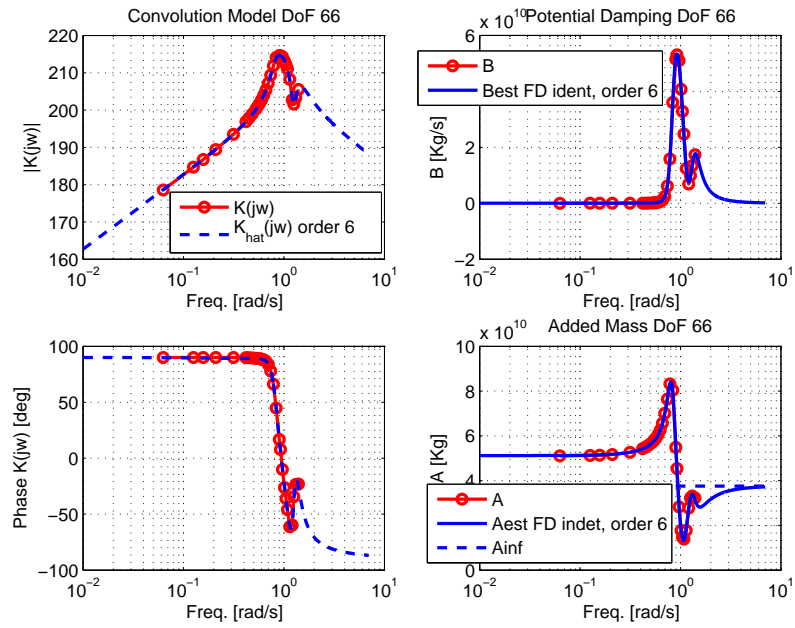


Figure 7: Data fit corresponding to the coupling 6-6 of a semi-submersible. The left hand side plots show the magnitude and phase of  $K_{66}(j\omega)$  and  $\hat{K}_{66}(j\omega)$  for a parametric approximation of order 6. The right-hand side plots show damping and added mass computed by the code and the approximations based on  $\hat{K}_{66}(j\omega)$ .

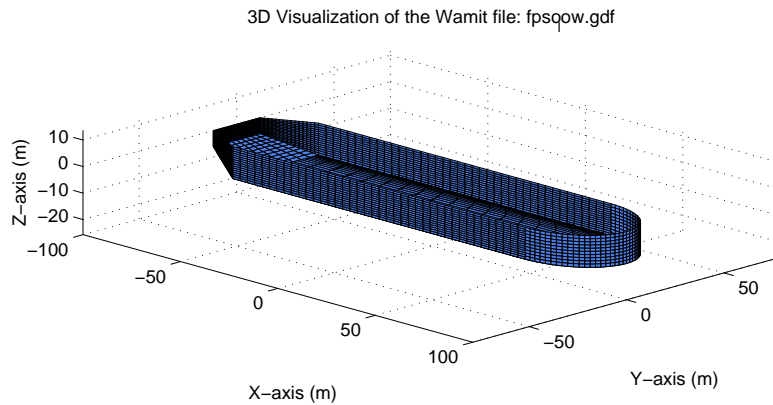


Figure 8: Hull geometry of a FPSO. Data from [www.marinecontrol.org](http://www.marinecontrol.org)

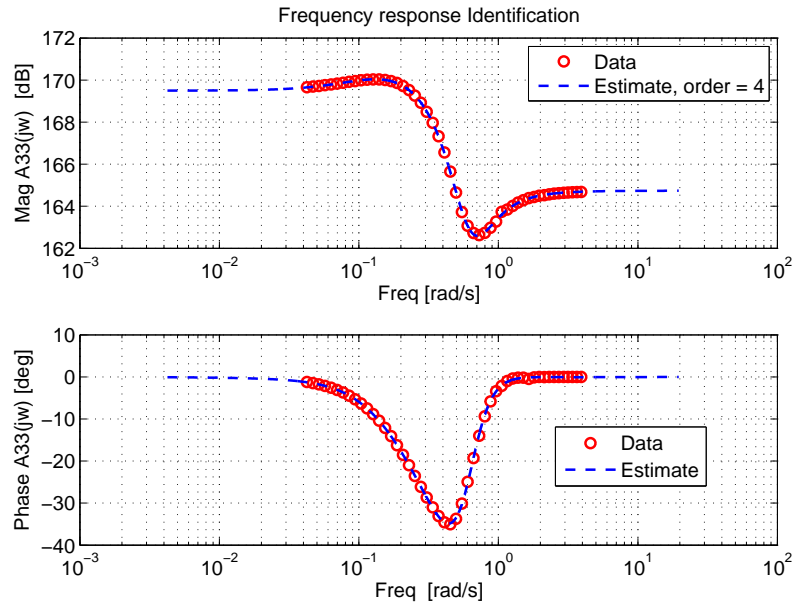


Figure 9: Data fit of the complex coefficient  $\tilde{A}_{33}(j\omega)$  of a FPSO with a parametric model of order 4.

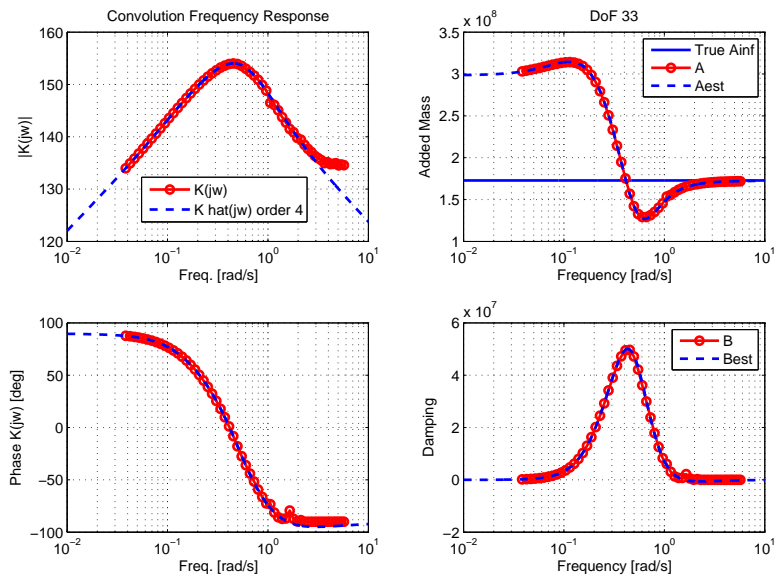


Figure 10: Data fit of  $A_{\infty,33}$  and  $K_{33}(j\omega)$  of a FPSO with a parametric model of order 4. The left-hand side column shows the magnitude and phase of  $K_{33}(j\omega)$  and  $\hat{K}_{33}(j\omega)$ . The right-hand plots show the frequency-dependant added mass and damping obtained from the identified fluid memory function  $\hat{K}_{33}(j\omega)$  together with  $A_{\infty,33}$  and  $\hat{A}_{\infty,33}$ .

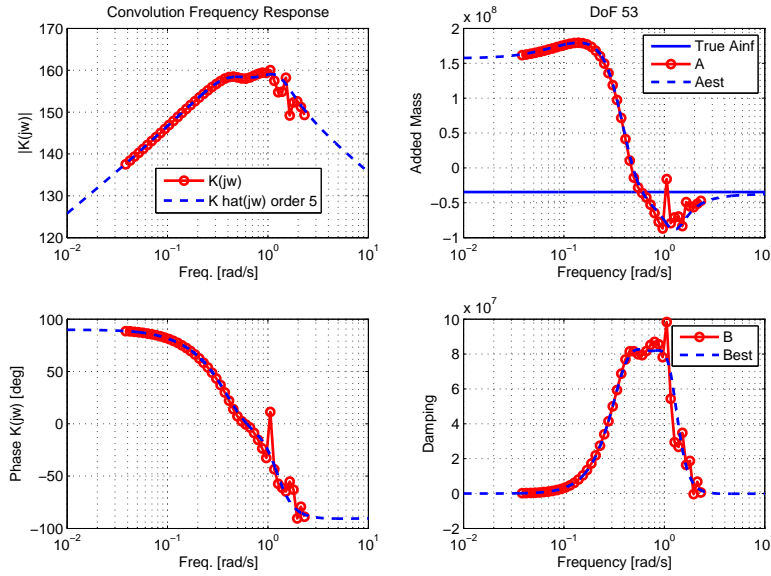


Figure 11: Data fit of  $A_{\infty,53}$  and  $K_{53}(j\omega)$  of a FPSO with a parametric model of order 5. The left-hand side column shows the magnitude and phase of  $K_{53}(j\omega)$  and  $\hat{K}_{53}(j\omega)$ . The right-hand plots show the frequency-dependant added mass and damping obtained from the identified fluid memory function  $\hat{K}_{53}(j\omega)$  together with  $A_{\infty,53}$  and  $\hat{A}_{\infty,53}$ .

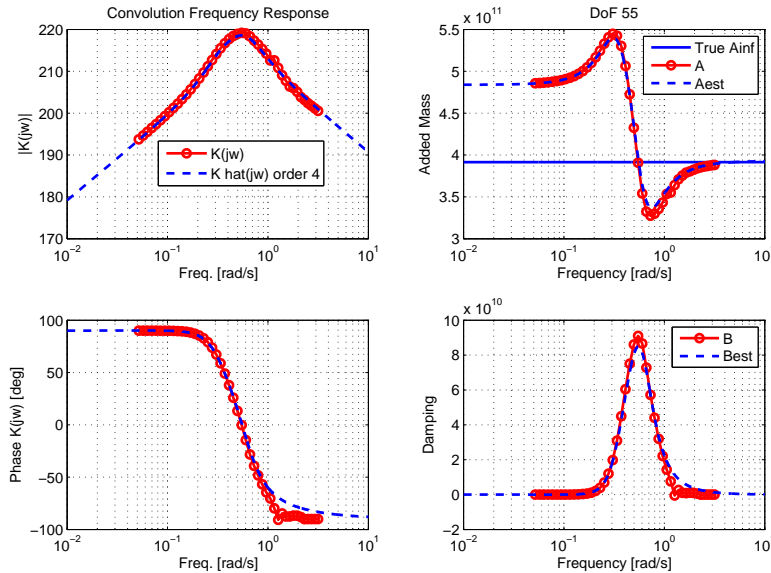


Figure 12: Data fit of  $A_{\infty,55}$  and  $K_{55}(j\omega)$  of a FPSO with a parametric model of order 4. The left-hand side column shows the magnitude and phase of  $K_{55}(j\omega)$  and  $\hat{K}_{55}(j\omega)$ . The right-hand plots show the frequency-dependant added mass and damping obtained from the identified fluid memory function  $\hat{K}_{55}(j\omega)$  together with  $A_{\infty,55}$  and  $\hat{A}_{\infty,55}$ .